# Anisotropic s-Wave Gap in the Vicinity of a Quantum Critical Point in Superconducting $BaFe_2(As_{1-x}P_x)_2$ Single Crystals: A Study of Point-Contact Spectroscopy

Hong-Xing Zhan(詹红星)[1], Yu-Chi Lin(林玉尺)[1], Yu-Qing Zhao(赵宇清)[1], Hai-Yan Zuo(左海艳)[1], Xing-Yu Wang(王兴玉)[2], Xiao-Yan Ma(马肖燕)[2], Chun-Hong Li(李春红)[2], Hui-Qian Luo(罗会仟)[2], Gen-Fu Chen(陈根富)[2], Shi-Liang Li(李世亮)[2*], and Cong Ren(任聪)[1,3*]

[1]*School of Physics and Astronomy, Yunnan University, Kunming 650500, China*
[2]*Beijing National Laboratory for Condensed Matter Physics, and Institute of Physics, Chinese Academy of Sciences, Beijing 100190, China*
[3]*Yunnan Key Laboratory for Electromagnetic Materials and Devices, Yunnan University, Kunming 650500, China*

(Received 15 January 2024; accepted manuscript online 2 April 2024)

We report on soft *c*-axis point-contact Andreev reflection (PCAR) spectroscopy combining with resistivity measurements on $BaFe_2(As_{0.7}P_{0.3})_2$, to elucidate the superconducting gap structure in the vicinity of the quantum critical point. A double peak at the gap edge plus a dip feature at zero-bias has been observed on the PCAR spectra, indicative of the presence of a nodeless gap in $BaFe_2(As_{0.7}P_{0.3})_2$. Detailed analysis within a sophisticated theoretical model reveals an anisotropic gap with deep gap minima. The PCARs also feature additional structures related to the electron–bosonic coupling mode. Using the extracted superconducting energy gap value, a characteristic bosonic energy $\Omega_b$ and its temperature dependence are obtained, comparable with the spin-resonance energy observed in neutron scattering experiment. These results indicate a magnetism-driven quantum critical point in the $BaFe_2(As_{1-x}P_x)_2$ system.

DOI: 10.1088/0256-307X/41/4/047402

As the second class of high-temperature superconductors (no inclusion of the recently discovered ultra high-pressure superconductors, such as $LaH_{10}$), iron-based superconductors provide new play grounds for investigating unconventional pairing mechanisms in high-$T_c$ superconductivity. One of the crucial issues to elucidate the mechanism leading to high-temperature superconductivity is the nature of pairing state, e.g., the symmetry and structure of the superconducting order parameter. Similar to high-$T_c$ cuprate superconductors, the iron-based superconductors bear a simultaneous presence of high-$T_c$ superconductivity and magnetism in the phase diagram, suggesting a spin-fluctuation-mediated superconductivity in iron pnictide superconductors.[1–4] On the basis of first-principle magnetic calculations, superconductivity in iron pnictides resulting from a superexchange repulsion mediated by magnetic excitations has been proposed, which couples electron and hole pockets of the Fermi surface (FS).[5,6] Such pairing interactions favor either isotropic s-wave order parameters with opposite signs on different sheets of the FS ($s_\pm$ model) or anisotropic s-wave or even d-wave order parameters with nodes.[6–11] On the other hand, observation of orbital-polarized state[12] stimulates theoretical studies of the orbital-fluctuation-mediated superconductivity, which favors a multiband s-wave pairing state without sign change, the $s_{++}$-wave model.[12–15]

While most of the experimental studies have so far indicated that the iron-based materials are a multiband system with nodeless $s_\pm$-wave superconducting pairing symmetry, some systems show signatures of nodes in the SC gap, such as LaFePO,[16] heavily hole-doped BaK-122, $K(Ca)Fe_2As_2$,[17,18] and isovalence doping system of $BaFe_2(As_{1-x}P_x)_2$.[19–21] Among the nodal SC compounds, the optimally isovalence-doped $BaFe_2(As_{0.7}P_{0.3})_2$ is particularly intriguing in that in the $BaFe_2(As_{1-x}P_x)_2$ system there exists a quantum critical point (QCP) with $x \simeq 0.3$.[21,22] This immediately raises the concerns on the gap structure in the vicinity of a QCP in iron pnictide superconductor.[23] In $BaFe_2(As_{1-x}P_x)_2$, penetration depth and thermal conductivity measurements claimed a robust nodal gap in the whole doping region.[19,21] Nuclear magnetic resonance results show the existence of a residual density of state at zero energy in $BaFe_2(As_{0.68}P_{0.32})_2$, consistent with the presence of nodes in the SC gap.[24] Angle resolved thermal conductivity measurement on $BaFe_2(As_{0.67}P_{0.33})_2$ also confirmed the closed nodal loops at the flat part of the electron FS.[25] Angle resolved photoemission (ARPES) experiments observed either a horizontal line node on the hole FSs[20] or a strongly anisotropic gap in the electron FS and an isotropic gap on the entire hole FSs.[26] These results are consistent with modified $s_\pm$ gap with nodal loops.[11] On the contrary, a high-resolution specific heat measurement on single crystal of $BaFe_2(As_{0.68}P_{0.32})_2$ revealed a nodeless gap.[27] Point

*Corresponding authors. Email: slli@iphy.ac.cn; cren@ynu.edu.cn
© 2024 Chinese Physical Society and IOP Publishing Ltd

contact Andreev-reflection (PCAR) spectroscopy measurement on $BaFe_2(As_{1-x}P_x)_2$ thin film with a $T_c \simeq 30$ K have provided evidence for the possible presence of nodeless gap.[28] What is more, addition of disorder/impurity can lift the nodes in nodal s-wave SCs,[29] leading to a nodal-nodeless gap structure transition in the vicinity of a quantum critical point in $BaFe_2(As_{1-x}P_x)_2$.[30,31] These studies with different conclusions reflect the complexity of the system, and systematic investigations on high-quality samples using different techniques are highly desired.

Point-contact Andreev reflection (PCAR) spectroscopy, to some extent equivalent to tunneling spectroscopy, has been proven to be one of the most powerful tools in investigation of unconventional superconductors with a high energy resolution. Based on some sophisticated theoretical models, PCAR spectra have also been proven to be suitable to study unconventional superconductors with "exotic" properties such as anisotropic, nodal/nodeless, and multiple SC gaps. In addition, the capability of this technique to probe the electronic excitations makes it an important tool in providing invaluable information for various mechanisms of unconventional superconductivity.[32] In this work, we fabricate highly transparent $c$-axis direct contacts to perform the PCAR spectroscopy study on optimally isovalent doping $BaFe_2(As_{0.7}P_{0.3})_2$ single crystals. These $c$-axis conductance spectra clearly feature the presence of a nodeless gap and conductance peaks possibly related to an electron–bosonic coupling mode. By using a generalized two-gap Blonder–Tinkham–Klapwijk (BTK) model, we estimate the gap anisotropy and gap amplitude, and thus the bosonic energy $\Omega_b$. These results on $BaFe_2(As_{0.7}P_{0.3})_2$ shed light on the gap structure of $BaFe_2(As_{1-x}P_x)_2$ in the vicinity of a QCP.

Single crystals of $BaFe_2(As_{1-x}P_x)_2$ under investigation were grown through a $Ba_2As_3/Ba_2P_3$ flux method. Details for the growth process and sample characterization were published elsewhere.[33] The composition value $x = 0.3$ was determined using energy-dispersive electron-probe microanalysis (EDX). The in-plane electrical resistance was measured using a standard four-probe ac technique on Oxford instrument $^3$He cryostat with a 12 T magnet.

We have utilized point contact Andreev reflection spectroscopy (PCARS) technique to study the gap symmetry of the $BaFe_2(As_{0.7}P_{0.3})_2$ single crystals. In order to form the point contact configuration, we adopted a 'soft' point-contact technique,[34] in which a tiny Pt wire ($\phi = 16\,\mu$m) dipped in a thin drop of silver paste (4929N DuPont) with a size of about a few hundreds of microns was combined with a fresh shiny $BaFe_2(As_{0.7}P_{0.3})_2$ single crystal surface that cleaved with scalpel along the $c$-direction. Under the microscope, the typical size of these planar contacts is about 80–150 μm. For the back side of the wire, we covered the entire bottom area of the crystal with silver paste. Due to the nanoparticle nature of silver paste, contacts made in this manner are actually formed by many nanocontacts analogous to the tip-point contact technique.[34] The differential conductance $G(V) \equiv dI/dV(V)$ of the PCARS was recorded by sweeping the dc current source (Keysight B2901A) $I$ on which a small ac current $i$ is provided throughout a lock-in amplifier system (MFLI) that was superimposed using a standard lock-in technique. The measurements were also performed on the Oxford instrument $He^3$ cryostat with the temperature range from about 1.5 K to 300 K.

First we examine the nature of the quantum criticality in our samples by examining $T$-dependence of the normstate resistivity $\rho(T)$ in the whole $T$ range. As shown in the main panel of Fig. 1, the normal state resistivity decreases smoothly with temperature and no SDW-associated or/and structural transition-associated anomalies are observed in such $\rho(T)$ curves. As the temperature is lowered further, a very sharp superconducting transition appears. The sample enters zero resistivity state at 29.2 K. The superconducting transition width $\Delta T_c$ is about 0.96 K. The residue resistance ratio $\mathrm{RRR} \equiv R(300\,\mathrm{K})/R(0\,\mathrm{K}) = 10.2$, as the same value as other $x \simeq 0.30$ samples reported.[35,36]

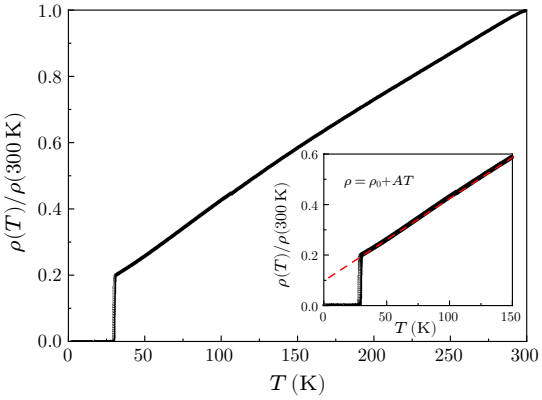


**Fig. 1.** Temperature dependence of in-plane resistivity $\rho(T)$ for $BaFe_2(As_{0.70}P_{0.30})_2$ single crystal. The $\rho(T)$ data are normalized by the value at $T = 300$ K. The inset shows the detailed $\rho(T)$ curve at $T < 150$ K. The dashed red line shows the fit to normal-state $\rho(T)$.

As shown in the inset of Fig. 1, $\rho(T)$ follows a perfect $T$-linear relationship in a wide $T$ range of 30–150 K as $\rho(T) = \rho_0 + AT$, where $A$ is a constant, $\rho_0$ is residual resistivity due to scattering on impurities and defects. Here, the $T$-linear $\rho(T)$ is argued to be a hallmark of non-Fermi liquid behavior, and regarded as the signature of the presence of quantum criticality. In particular, Kasahara *et al.*[21] proven that for the $BaFe_2(As_{1-x}P_x)_2$ system, there exists a quantum critical point at $x \simeq 0.3$ in the phase diagram. Thus, the normal state transport property is consistent with the presence of a QCP in our $BaFe_2(As_{0.7}P_{0.3})_2$ crystals.

Figures 2(a) and 2(b) present the typical raw conductance curves $G(V) = dI(V)/dV$ of $c$-axis $Ag/BaFe_2(As_{0.7}P_{0.3})_2$ contacts 1 and 2 at various $T$, respectively. These $T$-dependent $G(V)$ curves show clear Andreev reflection features in the form of a conductance enhancement around low bias. At high bias (in normal-state) these conductance curves are almost overlapped together, independent of $T$. These $T$-independent high bias

$G(V)$ implies that there are no other conducting channels for electron transport through Ag-$BaFe_2(As_{0.7}P_{0.3})_2$ interface, suggesting that these conducting contacts are in ballistic regime in momentum space. Furthermore, the Andreev temperature $T_c^A$ defined as the gap opening/closing temperature exactly matches the superconducting resistive transition temperature $T_c^R$, as shown in Figs. 2(c) and 2(d) for contacts 1 and 2, respectively. There is no sign of spectroscopic anomalies associated to the breakdown of superconductivity[37] so that one can rather safely assume that the contacts are in the spectroscopic regime, thus, energy-resolved spectroscopy is possible. On the aspects of unconventionality of the Andreev conductance spectra, it is worth noting that there is a pair of slightly asymmetric coherence peaks at low bias relating to the underlying superconductivity. Both the asymmetric coherence peak and the broad humps in the normal-state $G_N(V)$ have been widely observed in electron-correlation systems, such as cuprate,[38] heavy Fermion,[39] and iron pnictide superconductors.[28] In the present case, we surmise that both the asymmetric coherence peak and the broad humps might be an indicator of electron-correlation effect in $BaFe_2(As_{0.7}P_{0.3})_2$, consistent with the effective mass enhancement in the vicinity of a QCP of the $BaFe_2(As_{1-x}P_x)_2$ system.[40]

A feature in these $G(V)$ curves is that at low $T$ there exist well-defined double peaks at the gap-edge plus a "dip" structure at zero bias. In principle, the double peaks plus the dip structure at zero bias is the tell-tale signature of a fully gapped s-wave-like nodeless gap with the peak-peak distance strongly relating to the superconducting gap value for these $c$-axis Andreev junctions. It is noted that we have measured more than 10 pieces of Ag/$BaFe_2(As_{0.7}P_{0.3})_2$ point-contact planar junctions. All $G(V)$ spectra show the identical "double peak, zero-bias dip" behavior. No clear sign of nodal gap was observed in these $c$-axis $G(V)$ spectra of $BaFe_2(As_{0.7}P_{0.3})_2$. We emphasize that the present observation of the absence of the nodal-gap superconductivity imposes a constraint on theoretical models for iron-based superconductivity in the vicinity of a QCP.

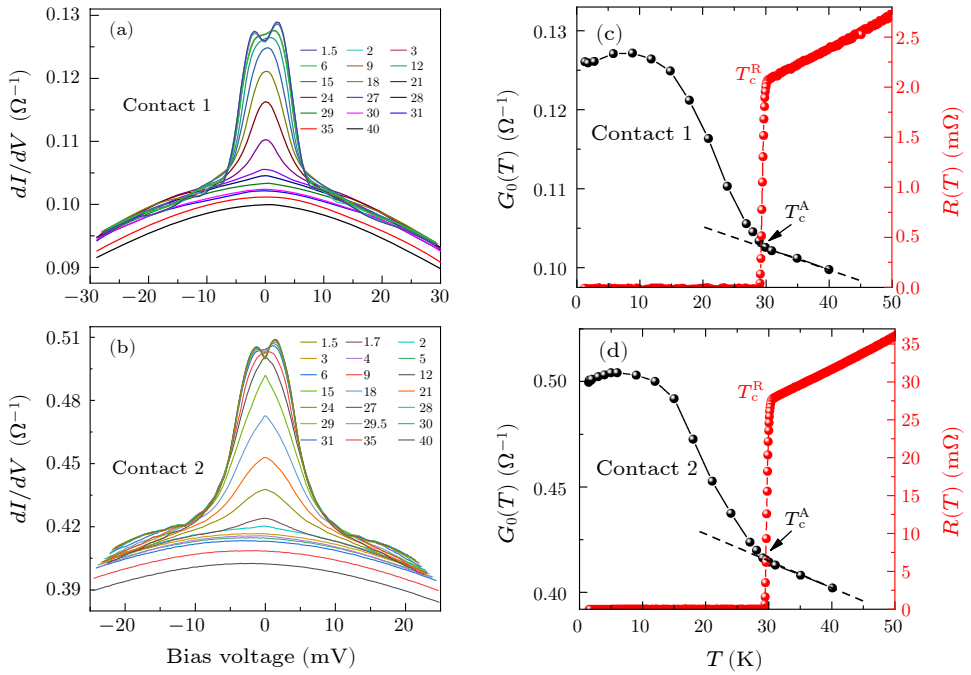


**Fig. 2.** Raw data of conductance spectra at various temperatures for $c$-axis Ag/$BaFe_2(As_{0.70}P_{0.30})_2$ (a) soft point contact 1 and (b) soft point contact 2. [(c), (d)] Temperature dependence of point-contact zero-bias conductance $G_0(T)$ in comparison with the in-plane electrical resistance for contacts 1 and 2, respectively. $T_c^A$ and $T_c^R$ stands for superconducting gap opening/closing temperature (Andreev temperature) and superconducting resistive transition temperature determined by $G_N(0)$ and in-plane resistivity, respectively.

To quantitatively elucidate the gap structure and gap amplitude of $BaFe_2(As_{1-x}P_x)_2$, we analyze the obtained $G(V)$ spectra by evoking the extended two-dimensional BTK model.[41,42] This model contains three fitting parameters: the gap amplitude $\Delta$, the transparency of barrier at the N/S (normal metal/superconductor) interface ($Z$), and the smearing parameter $\Gamma$.[43] Since the quasi-particle (QP) current is injected along the $c$-axis of $BaFe_2(As_{0.7}P_{0.3})_2$, we integrate the kernel $\sigma_S(E, \phi)$, over the full half of the momentum space:

$$\frac{dI}{dV} = \frac{\int_0^{2\pi} d\phi \int_0^{\pi/2} d\theta \int_{-\infty}^{\infty} dE \frac{df(E-eV)}{dV} \sigma_S(E, \phi) \sin(2\theta)}{\int_0^{2\pi} d\phi \int_0^{\pi/2} d\theta \sigma_N \sin(2\theta)}, \quad (1)$$

where $\sigma_S(E, \phi) = [1+|\Lambda|]^2+Z^2(1+|\Lambda|^4)/|1+Z^2(1-|\Lambda|^2)|^2$, $\Lambda = E' - \sqrt{E'^2 - |\Delta|^2}/|\Delta|$, $E' = E - i\Gamma$ items incorporate

a QP lifetime broadening, $\Gamma = \hbar/\tau$ is the QP scattering rate and takes the real part of the kernel, $\sigma_N = 1/(1+Z^2)$, and $Z = Z_{\rm eff}/\cos\theta$. Here $\Delta(T, \theta)$ is the general gap function. $\Delta(T, \theta)$ has different functions based on different gap structures. We list it (i) as a single s-wave gap $\Delta(T, \theta) = \Delta(T)$ and (ii) as a single anisotropic s-wave gap $\Delta(T, \theta) = \Delta_0(T)[1 + a\cos(2\theta)]$. Here, $a$ denotes the gap anisotropy. If $a = 1$, the gap function will be zero at some points, indicative of a nodal gap. When $a$ is close to 0, it means that the anisotropy is very small and the extended s-wave gap will degenerate into isotropic s-wave gap.

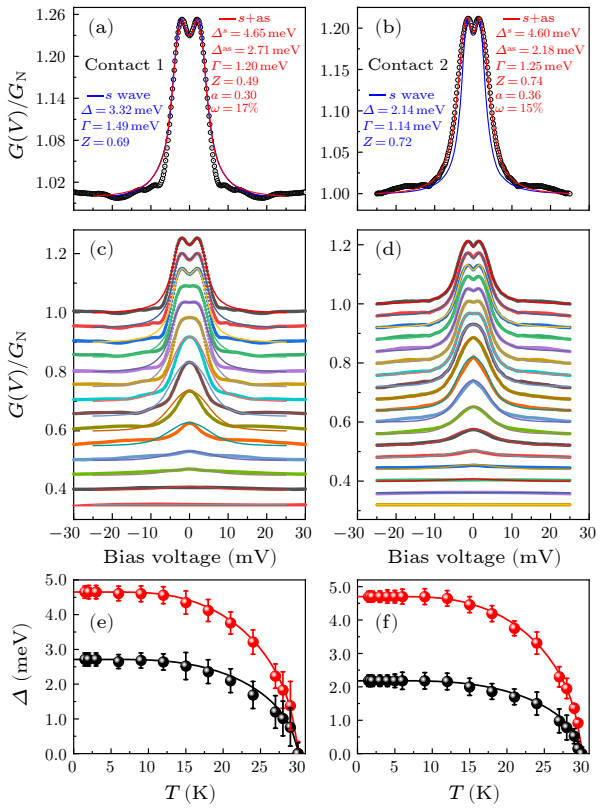


**Fig. 3.** [(a), (b)] Representative symmetrical normalized point-contact conductance curves $G(V)/G_N$ at 1.5 K for 1 and 2. The solid lines (red lines are two band fits and blue lines are single s-wave fits) are their BTK fits, with the relevant fitting parameters reported in labels. [(c), (d)] The normalized conductance spectra of the corresponding point contacts at various $T$, in comparison with two-band BTK fitting (solid lines), respectively. [(e), (f)] Temperature evolution of the extracted superconducting energy gap, with the solid lines standing for the BCS-like $\Delta(T)$ function.

We first adopt the simplest single s-wave model to describe the obtained $G(V)$ spectra. As shown in Fig. 3(a), the single s-wave gap can well fit the $G(V)$ data of 1. However, the fit-resulted gap amplitude $\Delta \simeq 3.32 \pm 0.05$ meV is relatively small compared to the BCS gap $\Delta_{\rm BCS} \simeq 4.48$ meV with $T_c \simeq 30.0$ K. This indicates the necessity of adopting a two-gap model. For contact 2, the single s-wave model even fits the $G(V)$ spectral data far from satisfactory, as shown by the blue curve in Fig. 3(b). The failure of the single s-wave model to fit the $G(V)$ spectra indicates the multi-gap character for $BaFe_2(As_{0.7}P_{0.3})_2$. Thus we adopt the two-gap BTK model with one gap being a fully gap and the other being an anisotropic gap: $G(V) = \omega G^{\rm s}(V) + (1-\omega)G^{\rm as}(V)$, in which $G^{\rm s}(V)$ represents the contribution from the s-wave gap and $G^{\rm as}(V)$ the contribution from the anisotropic gap with $\omega$ being the spectral weight. The solid red lines in Figs. 3(a) and 3(b) represent the best fits of the spectra for contacts 1 and 2 at lowest $T = 1.5$ K. The relevant fitting parameters are listed as $Z = 0.49$, $\Gamma = 1.20$ meV, $\Delta^{\rm s} \simeq 4.6$ meV, $\Delta^{\rm as} \simeq 2.7$ meV, $a \simeq 0.3$, and $\omega = 0.17$ for contact 1; $Z = 0.74$, $\Gamma = 1.25$ meV, $\Delta^{\rm s} \simeq 4.7$ meV, $\Delta^{\rm as} \simeq 2.2$ meV, $a \simeq 0.36$ and $\omega = 0.15$ for contact 2. It is notable that both the values of $\Gamma/\Delta^{\rm s}$ and $\Gamma/\Delta^{\rm as}$ for contacts 1 and 2 are less than 0.5, indicative of the rationality and reliability of our fit.

With these fitting parameters, we check the validity of these fits by extending the fit to the overall temperature spectra. As shown in Figs. 3(c) and 3(d), the two-gap model fits reasonably well the $T$-dependence of these $G(V)$ curves. In the whole $T$ region up to $T_c$, the $Z$ value slightly increases from 0.50 up to 0.65 and $\Gamma$ from 1.20 to 1.81 meV for contact 1. The same is true for contact 2. The corresponding $T$-dependent superconducting gaps $\Delta$ of contacts 1 and 2 extracted from the fitting are shown in Figs. 3(e) and 3(f) and they follow the BCS-like gap-$T$ function: $\Delta = \Delta_0 \tanh(\alpha\sqrt{T_c/T-1})$ for both $\Delta^{\rm s}$ and $\Delta^{\rm as}$. The zero-$T$ superconducting gaps $\Delta$ are extrapolated to be equal to those of lowest $T = 1.5$ K, and the corresponding $T_c \simeq 30$ K.

The fit-resulted gap size of $\Delta^{\rm s} \simeq 4.7$ meV is consistent with the gap size on the hole Fermi surfaces of $\sim 5$ meV observed in the ARPES experiment and in the optical transient reflectivity measurement on $BaFe_2(As_{0.7}P_{0.3})_2$ single crystals.[26,44] Specifically, according to the ARPES experiment, for the $\beta$ and $\gamma$ bands of hole FSs, the gap energies are 5–8 meV and are nearly isotropic on the entire hole FSs. On the contrary, a strong anisotropy in the SC gap was found on electron-like FSs.[26] Thus we attribute the obtained $\Delta^{\rm as} \sim 2.5$ meV to the anisotropic gap on the electron FSs with a deep gap minimum of 1.8–1.9 meV in this multiband system.

In addition to the spectral fit, another feature appears in these $G(V)$ curves just locating around the gap edge as a "peak-hump-dip" structure. As shown in Fig. 4(a), the conductance spectra of contact 1 shows the peak-hump-dip feature at about $E_p \sim 15$ meV by comparing the $G(V)$ spectra at lowest $T$ and normal-state $G(V)$ curve. Followed the case of strong coupling superconductor, Pb as the example, the peak-hump-dip is explicitly displayed as a peak in the form of the second derivative $-dI^2/dV^2$ at low $T$. Figure 4(b) shows $-d^2I/dV^2$ of contact 1 at lowest $T = 1.5$ K, PCAR spectra clearly show a main maxim at about $E_P \simeq 15$ meV. Accordingly, a characteristic energy, the electron–bosonic coupling energy $\Omega_b = E_p - \Delta^{\rm s} \simeq 10$ meV is extracted. This energy scale $\Omega_b$ is compatible with the spin resonance energy of 11 meV observed by neutron scattering experiment on a similar

sample.[45,46] In Fig. 4(c) we present the obtained $\Omega_b$ of our $BaFe_2(As_{0.7}P_{0.3})_2$ together with other iron pnictide superconductors, including BaK-122,[47] BaCo(Ni)-122,[48,49] Sm-1111, and FeSe for comparison. As is shown, $\Omega_b$ is well scaled with $T_c$ for all these iron pnictide superconductors as $\Omega_b \sim 4.3 k_B T_c$, in agreement with those results probed by neutron scattering experiments with a $\Omega_b$–$T_c$ empirical formula: $\Omega_b \simeq 4.6 \sim 4.9\, k_B T_c$.[50] These observations indicate that $BaFe_2(As_{0.7}P_{0.3})_2$ has similar characteristics to the iron-based Ba-122 superconducting systems. Thus our results, the multi-band superconductivity with an anisotropic superconducting gap and the electron–bosonic coupling mode associated with the spin resonant excitation in energy scale, strongly support the pairing interaction mediated by the antiferromagnetic spin fluctuations in the vicinity of a QCP in the $BaFe_2(As_{1-x}P_x)_2$ system.

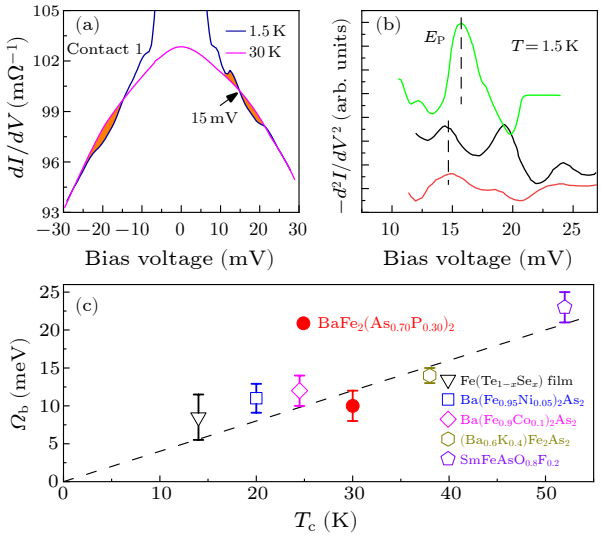


**Fig. 4.** (a) The raw conductance spectra $G(V)$ at lowest $T$ and $T_c$ to show the "hump" structure at the gap edge. (b) Three samples show the hump structure in the form of the second derivative $-d^2I/dV^2$ curves at the lowest $T$. (c) Correlations between the bosonic energies $\Omega_b$ and $T_c$ in some typical iron pnictide superconductors.

In summary, we have performed soft PCAR spectroscopy combining with electrical transport measurements on superconducting $BaFe_2(As_{0.7}P_{0.3})_2$ single crystals. The $T$-dependence of the resistivity indicates the presence of a QCP in the $BaFe_2(As_{1-x}P_x)_2$ phase diagram. A typical double-peak plus "dip" structure around low bias is observed in the PCAR spectroscopy, a tell-tale signature of a nodeless gap in $BaFe_2(As_{0.7}P_{0.3})_2$. Normalized Andreev conductance $G(V)/G_N$ curves can be well fitted by a two-gap BTK model with at least one anisotropic superconducting gap with deep gap minima. Moreover, additional energy mode related to electron–bosonic coupling is observed, and the characteristic energy of mediating boson, $\Omega_b \simeq 10$ meV, is compatible with the spin-resonance mode observed in neutron scattering experiments. Therefore, these results support a dominance of spin fluctuation mediated mechanism of pairing state for $BaFe_2(As_{0.7}P_{0.3})_2$.

*Acknowledgements.* C.R. expresses gratitude to Professor Hai-Hu Wen for insightful discussion. This work was supported by the National Natural Science Foundation of China (Grant Nos. 11774303 and 11574373), the National Key Research and Development Program of China (Grant Nos. 2022YFA1403402, 2021YFA1400401, and 2020YFA0406003), and the Chinese Academy of Sciences (Grant Nos. XDB33000000 and GJTD-2020-01). C.R. acknowledges financial support from the Joint Fund of Yunnan Provincial Science and Technology Department (Grant No. 2019FY003008).

# References

[1] Johnston D C 2010 *Adv. Phys.* **59** 803
[2] Stewart G R 2011 *Rev. Mod. Phys.* **83** 1589
[3] Hirschfeld P J, Korshunov M M, and Mazin I I 2011 *Rep. Prog. Phys.* **74** 124508
[4] Chubukov A 2012 *Annu. Rev. Condens. Matter Phys.* **3** 57
[5] Mazin I I, Singh D J, Johannes M D, and Du M H 2008 *Phys. Rev. Lett.* **101** 057003
[6] Boeri L, Dolgov O V, and Golubov A A 2008 *Phys. Rev. Lett.* **101** 026403
[7] Kuroki K, Onari S, Arita R, Usui H, Tanaka Y, Kontani H, and Aoki H 2008 *Phys. Rev. Lett.* **101** 087004 Erratum: 2009 *Phys. Rev. Lett.* **102** 109902
[8] Wang F, Zhai H, Ran Y, Vishwanath A, and Lee D H 2009 *Phys. Rev. Lett.* **102** 047005
[9] Maier T A, Graser S, Scalapino D J, and Hirschfeld P J 2009 *Phys. Rev. B* **79** 224510
[10] Graser S, Kemper A F, Maier T A, Cheng H P, Hirschfeld P J, and Scalapino D J 2010 *Phys. Rev. B* **81** 214503
[11] Nakaoka H, Yamakawa Y, and Kontani H 2018 *Phys. Rev. B* **98** 125107
[12] Shimojima T, Ishizaka K, Ishida Y, Katayama N, Ohgushi K, Kiss T, Okawa M, Togashi T, Wang X Y, Chen C T, Watanabe S, Kadota R, Oguchi T, Chainani A, and Shin S 2010 *Phys. Rev. Lett.* **104** 057002
[13] Kontani H and Onari S 2010 *Phys. Rev. Lett.* **104** 157001
[14] Saito T, Onari S, and Kontani H 2010 *Phys. Rev. B* **82** 144510
[15] Zhang J, Sknepnek R, Fernandes R M, and Schmalian J 2009 *Phys. Rev. B* **79** 220502
[16] Fletcher J D, Serafin A, Malone L, Analytis J G, Chu J H, Erickson A S, Fisher I R, and Carrington A 2009 *Phys. Rev. Lett.* **102** 147001
[17] Okazaki K, Ota Y, Kotani Y, Malaeb W, Ishida Y, Shimojima T, Kiss T, Watanabe S, Chen C T, Kihou K, Lee C H, Iyo A, Eisaki H, Saito T, Fukazawa H, Kohori Y, Hashimoto K, Shibauchi T, Matsuda Y, Ikeda H, Miyahara H, Arita R, Chainani A, and Shin S 2012 *Science* **337** 1314
[18] Gonnelli R S, Daghero D, Tortello M, Ummarino G A, Bukowski Z, Karpinski J, Reuvekamp P G, Kremer R K, Profeta G, Suzuki K, and Kuroki K 2016 *Sci. Rep.* **6** 26394
[19] Hashimoto K, Yamashita M, Kasahara S, Senshu Y, Nakata N, Tonegawa S, Ikada K, Serafin A, Carrington A, Terashima T, Ikeda H, Shibauchi T, and Matsuda Y 2010 *Phys. Rev. B* **81** 220501
[20] Zhang Y, Ye Z R, Ge Q Q, Chen F, Jiang J, Xu M, Xie B P, and Feng D L 2012 *Nat. Phys.* **8** 371
[21] Hashimoto K, Cho K, Shibauchi T, Kasahara S, Mizukami Y, Katsumata R, Tsuruhara Y, Terashima T, Ikeda H, Tanatar M A, Kitano H, Salovich N, Giannetta R W, Walmsley P, Carrington A, Prozorov R, and Matsuda Y 2012 *Science* **336** 1554

[22] Shibauchi T, Carrington A, and Matsuda Y 2014 *Annu. Rev. Condens. Matter Phys.* **5** 113
[23] Huang H X, Li W, Gao Y, Chen Y, and Zhang F C 2019 *Phys. Rev. B* **100** 144501
[24] Nakai Y, Iye T, Kitagawa S, Ishida K, Kasahara S, Shibauchi T, Matsuda Y, and Terashima T 2010 *Phys. Rev. B* **81** 020503
[25] Yamashita M, Senshu Y, Shibauchi T, Kasahara S, Hashimoto K, Watanabe D, Ikeda H, Terashima T, Vekhter I, Vorontsov A B, and Matsuda Y 2011 *Phys. Rev. B* **84** 060507
[26] Yoshida T, Ideta S, Shimojima T, Malaeb W, Shinada K, Suzuki H, Nishi I, Fujimori A, Ishizaka K, Shin S, Nakashima Y, Anzai H, Arita M, Ino A, Namatame H, Taniguchi M, Kumigashira H, Ono K, Kasahara S, Shibauchi T, Terashima T, Matsuda Y, Nakajima M, Uchida S, Tomioka Y, Ito T, Kihou K, Lee C H, Iyo A, Eisaki H, Ikeda H, Arita R, Saito T, Onari S, and Kontan H 2014 *Sci. Rep.* **4** 7292
[27] Diao Z, Campanini D, Fang L, Kwok W K, Welp U, and Rydh A 2016 *Phys. Rev. B* **93** 014509
[28] Daghero D, Tortello M, Ummarino G A, Piatti E, Ghigo G, Hatano T, Kawaguchi T, Ikuta H, and Gonnelli R S 2018 *Supercond. Sci. Technol* **31** 034005
[29] Wang Y, Kreisel A, Hirschfeld P J, and Mishra V 2013 *Phys. Rev. B* **87** 094504
[30] Mizukami Y, Konczykowski M, Kawamoto Y, Kurata S, Kasahara S, Hashimoto K, Mishra V, Kreisel A, Wang Y, Hirschfeld P J, Matsuda Y, and Shibauchi T 2014 *Nat. Commun.* **5** 5657
[31] Mizukami Y, Konczykowski M, Matsuura K, Watashige T, Kasahara S, Matsuda Y, and Shibauchi T 2017 *J. Phys. Soc. Jpn.* **86** 083706
[32] Daghero D, Tortello M, Ummarino G A, and Gonnelli R S 2011 *Rep. Prog. Phys.* **74** 124509
[33] Nakajima M, Uchida S I, Kihou K, Lee C H, Iyo A, and Eisaki H 2012 *J. Phys. Soc. Jpn.* **81** 104710
[34] Gonnelli R S, Daghero D, Ummarino G A, Stepanov V A, Jun J, Kazakov S M, and Karpinski J 2002 *Phys. Rev. Lett.* **89** 247004
[35] Ye Z R, Zhang Y, Chen F, Xu M, Ge Q Q, Jiang J, Xie B P, and Feng D L 2012 *Phys. Rev. B* **86** 035136
[36] Analytis J G, Kuo H H, McDonald R D, Wartenbe M, Rourke P M C, Hussey N E, and Fisher I R 2014 *Nat. Phys.* **10** 194
[37] Howlader S and Sheet G 2021 *J. Phys.: Condens. Matter* **33** 403002
[38] Shan L, Huang Y, Wang Y L, Li S L, Zhao J, Dai P C, Zhang Y Z, Ren C, and Wen H H 2008 *Phys. Rev. B* **77** 014526
[39] Park W K, Sarrao J L, Thompson J D, and Greene L H 2008 *Phys. Rev. Lett.* **100** 177001
[40] Grinenko V, Iida K, Kurth F, Efremov D V, Drechsler S L, Cherniavskii I, Morozov I, Hänisch J, Föster T, Tarantini C, Jaroszynski J, Maiorov B, Jaime M, Yamamoto A, Nakamura I, Fujimoto R, Hatano T, Ikuta H, and Hühne R 2017 *Sci. Rep.* **7** 4589
[41] Blonder G E, Tinkham M, and Klapwijk T M 1982 *Phys. Rev. B* **25** 4515
[42] Tanaka Y and Kashiwaya S 1995 *Phys. Rev. Lett.* **74** 3451
[43] Dynes R C, Narayanamurti V, and Garno J P 1978 *Phys. Rev. Lett.* **41** 1509
[44] Pogrebna A, Mertelj T, Ye Z R, Feng D L, and Mihailovic D 2015 *Phys. Rev. B* **92** 144503
[45] Hu D, Zhang W L, Wei Y, Roessli B, Skoulatos M, Regnault L P, Chen G F, Song Y, Luo H Q, Li S L, and Dai P C 2017 *Phys. Rev. B* **96** 180503
[46] Ishikado M, Nagai Y, Kodama K, Kajimoto R, Nakamura M, Inamura Y, Wakimoto S, Nakamura H, Machida M, Suzuki K, Usui H, Kuroki K, Iyo A, Eisaki H, Arai M, and Shamoto S 2011 *Phys. Rev. B* **84** 144517
[47] Shan L, Gong J, Wang Y L, Shen B, Hou X Y, Ren C, Li C H, Yang H, Wen H H, Li S L, and Dai P C 2012 *Phys. Rev. Lett.* **108** 227002
[48] Tortello M, Daghero D, Ummarino G A, Stepanov V A, Jiang J, Weiss J D, Hellstrom E E, and Gonnelli R S 2010 *Phys. Rev. Lett.* **105** 237002
[49] Wang Z S, Wang Z Y, Luo H Q, Lu X Y, Zhu J, Li C H, Shan L, Yang H, Wen H H, and Ren C 2012 *Phys. Rev. B* **86** 060508
[50] Hong W S, Song L X, Liu B, Li Z Z, Zeng Z Y, Li Y, Wu D S, Sui Q T, Xie T, Danilkin S, Ghosh H, Ghosh A, Hu J P, Zhao L, Zhou X J, Qiu X G, Li S L, and Luo H Q 2020 *Phys. Rev. Lett.* **125** 117002